



1 **Assessing tropical cyclone compound flood risk using hydrodynamic**
2 **modelling: a case study in Haikou City, China**

3 **Qing Liu, Hanqing Xu, Jun Wang***

4 Key Laboratory of Geographic Information Science of Ministry of Education, School of
5 Geographic Science, East China Normal University, Shanghai, 200241, China

6 *Corresponding author.

7 Email address: uniqliu@163.com (Q. Liu), xuhq@stu.ecnu.edu.cn (H.Q. Xu),
8 jwang@geo.ecnu.edu.cn (J. Wang).

9
10 **Abstract** The co-occurrence of storm tide and rainstorm during tropical cyclones (TCs) can lead
11 to compound flooding in low-lying coastal regions. The assessment of TC compound flood risk
12 can provide vital insight for research on coastal flooding prevention. This study investigates TC
13 compound flooding by constructing a storm surge model and overland flooding model using
14 Delft3D Flexible Mesh (DFM), illustrating the serious consequences from the perspective of
15 storm tide. Based on the probability distribution of storm tide, this study regards TC1415 as the
16 100-year event, TC6311 as the 50-year event, TC8616 as the 25-year event, TC8007 as the
17 10-year event, and TC7109 as the 5-year event. The results indicate that the coastal area is a major
18 floodplain, primarily due to storm tide, with the inundation severity positively correlated with the
19 height of the storm tide. For 100-year TC event, the inundation area with a depth above 1.0 m
20 increases by approximately 2.5 times when compared with 5-year TC event. The comparison of
21 single-driven flood (storm tide flooding and rainstorm inundation) and compound flood hazards
22 shows that simply accumulating every single-driven flood hazard to define the compound flood
23 hazard may cause underestimation. For future research on compound flooding, copula function
24 can be adopted to investigate the joint occurrence of storm tide and rainstorm to reveal the severity
25 of extreme TC flood hazards.

26 **Keywords** Tropical cyclones; Compound flooding; Storm tide; Rainstorm; Coastal cities

27



28 **1 Introduction**

29

30 Flood hazards, especially those happening during tropical cyclones (TCs), have become the most
31 devastating and expensive natural hazards of coastal cities (Patricola and Wehner, 2018; van
32 Oldenborgh et al., 2017; Hallegatte et al., 2013; Adelekan, 2011). Storm tides brought on by TCs
33 can lead to coastal flooding, and rainstorms occurring during TCs can lead to urban inundation.
34 The simultaneous or consecutive occurrence of storm tide and rainstorm in time and/or space can
35 lead to compound flooding (Gori et al., 2020b; Wahl et al., 2015; Leonard et al., 2014). In the past
36 decade, many compound flood hazards occurred in coastal regions worldwide due to TCs, such as
37 Typhoon Irma (2017) in Jacksonville and Typhoon Lekima on China's southeast coast. An
38 extremely destructive flood event in Houston-Galveston during Hurricane Harvey (2017) was
39 confirmed to be a compound flood hazard (Huang et al., 2021). It was caused by land-derived
40 runoff (mainly considered to be rainfall) and ocean-derived forcing (mainly considered to be storm
41 tide) (Valle-Levinson et al., 2020). The coastal region suffered a major economic loss of more than
42 125 billion dollars from Harvey. Thus, it is important to investigate the compound flood risk
43 during TCs to better comprehend flood hazards in coastal cities.

44

45 The projection of future climate change indicates that TCs will occur more frequently with greater
46 intensity. Accordingly, the likelihood of the co-occurrence of storm tide and rainstorm will
47 increase drastically (Keellings and Hernández Ayala, 2019; Marsooli et al., 2019; Emanuel, 2017;
48 Lin et al., 2012), which may cause more extreme compound flood hazards (Bevacqua et al., 2019;
49 Rasmussen et al., 2017; Wahl et al., 2015; Milly et al., 2002). Due to global warming, sea level
50 rise, land subsidence, and urban expansion, coastal cities are confronted with the critical threat of
51 TC compound flooding (Yin et al., 2021, 2020; Wang and Tan, 2021; Hsiao et al., 2021; Wang et
52 al., 2018). Recent studies evaluated compound flood risk at the regional scale (Fang et al., 2020;
53 Bevacqua et al., 2019; Hendry et al., 2019; Budiyono et al., 2016; Wahl et al., 2015). Wahl et al.
54 (2015) assessed the risk of compound flooding from rainfall and storm surge in major US cities.
55 Bevacqua et al. (2019) estimated the probability of compound flooding from precipitation and
56 storm surge in Europe. Both studies showed that there will be an increase of compound flood risk
57 in coastal cities in the future. A study conducted by Fang et al. (2020) investigated the compound
58 flood potential from precipitation and storm surge in coastal China, indicating that low-latitude
59 (<30°N) coastal areas in southeast China are more prone to compound flood hazards from storm
60 tide and rainfall during TCs.

61

62 Only several urban-scale studies on compound flooding have been carried out in China (He et al.,
63 2020; Wang et al., 2019; Xu et al., 2018; Yin et al., 2016). Lian et al. (2013) investigated the joint
64 impact of rainfall and tidal level on flood risk in Fuzhou City. Xu et al. (2014) analyzed the joint
65 probability of rainfall and storm tide under changing environment, concluding that the probability



66 of compound flooding would increase by more than 300% in Fuzhou. Lian et al. (2017) identified
67 the major hazard-causing factors of compound flooding and classified the floodplains into tidal
68 zone, hydrological zone, and transition zone in Haikou City. Although studies such as these have
69 investigated the joint risk of hazard-causing factors in compound floods, they seldom pay attention
70 to the compound flooding that occurs during TCs.

71

72 Most studies concerned with compound flooding rely on historical data, which contains
73 information on hourly storm tide and daily rainfall (Yum et al., 2021; Fang et al., 2020; Zellou and
74 Rahali, 2019; Wu et al., 2018; Lian et al., 2017). The recorded data is often used to investigate the
75 statistical correlation between flood drivers (Xu et al., 2019, 2014; Xu et al., 2018; Lian et al.,
76 2013). Based on the recorded storm tide from 49 tide gauges and daily precipitation from 4890
77 rainfall stations in Australia, Zheng et al. (2013) quantified the dependence between rainfall and
78 storm surge to investigate flood risk in coastal zones. However, for a number of coastal regions in
79 the world, it is difficult to obtain sufficient recorded data that can be used to analyze the
80 mechanism of TC compound flooding from storm tide and rainfall. An alternative approach is
81 applying a hydrodynamic model to simulate storm tides (Gori et al., 2020a). For example, Yin
82 et al. (2021) constructed a storm surge model to simulate the storm tide derived from 5000 synthetic
83 TCs for the estimation of TC-induced coastal flood inundation.

84

85 Hydrodynamic models can also be employed to simulate flood events (Bevacqua et al., 2019;
86 Zellou and Rahali, 2019; Kumbier et al., 2018). It is an effective method to model the flood extent
87 and inundation depth, this method has generally been applied in research on single-driven flood
88 hazard (Wang et al., 2018, 2012; Yin et al., 2013). Recently, many studies have used
89 hydrodynamic models to simulate compound flood events driven by historical TC events or
90 synthetic TC scenarios (Bilskie et al., 2021; Orton et al., 2020; Santiago-Collazo et al., 2019; Shen
91 et al., 2019). Gori et al. (2020b) constructed a coupled framework of three models to simulate
92 storm surges and compound flood events. This method has the advantage of observing the
93 spatiotemporal dynamics of rainfall and storm surges during TCs (Gori et al., 2020b; Orton et al.,
94 2020). However, assessing the compound flood risk by constructing a coupled model is not
95 commonly used in current studies on compound flood hazards, mainly because the simulation of
96 compound flooding involves multiple driving condition settings and requires combining multiple
97 physics-based models.

98

99 Delft3D Flexible Mesh (DFM), developed by Deltares, Netherland, has been widely applied to
100 build storm surge numerical models for research on storm surge because of its capability of
101 simulating 2D and 3D shallow water flow (De Goede, 2020). It integrates Delft3D-FLOW model
102 suites and uses flexible unstructured grids, which is convenient for partial grid refinement
103 (Deltares, 2018). A recent study on compound flooding utilized this model to simulate storm



104 surges for characterizing extreme sea level, investigating the probability of compound floods from
105 precipitation and storm surge in Europe (Bevacqua et al., 2019). Meijer and Hutten (2018)
106 developed a 2D urban model with DFM for the downtown area of Shanghai. The results indicated
107 that DFM was capable of modeling rainfall-runoff and could be used to construct urban flood
108 models. Therefore, it is feasible to simulate both storm surge and rainfall-runoff based on DFM to
109 assess compound flooding.

110

111 This study investigates the compound effect of flooding from storm tide and rainstorm during TCs
112 to better understand of compound flooding in Haikou. Based on the DFM model, we set up a
113 storm surge model and overland flooding model to simulate the floodplain under TC events. We
114 select 66 TC events that influenced Haikou to explore the probability distribution of storm tide,
115 further selecting 5 TC events that respectively corresponds to the 5-, 10-, 25-, 50-, and 100-year
116 return period. The risk of rainstorm inundation, storm tide flooding, and compound flooding are
117 quantitatively assessed and compared based on the simulation results under different return periods.
118 The conclusions drawn from this study can provide insight into mitigating compound flood risk in
119 coastal areas.

120

121 To the best of our knowledge, this is the first study that applies a coupled model by DFM to assess
122 TC compound flood risk in Haikou. The objectives of this study include (1) investigating the
123 probability of storm tide during TCs by modelling TCs influenced Haikou; (2) quantifying the
124 compound effects of rainfall and storm surge under TC events of different return periods; (3)
125 assessing and comparing the flood severity of rainstorm inundation, storm tide flooding, and
126 compound flooding.

127

128 This paper is organized as follows: Section 2 presents the background information about the study
129 area and data requirements. Section 3 describes the model configuration and explains how TCs
130 that influenced Haikou were selected. The method of how to assess the compound flood risk is
131 also in this section. Model verification and the analysis of probability distribution of storm tide are
132 reported and discussed in Section 4. The assessment and comparison of rainstorm inundation,
133 storm tide flooding, and compound flooding are also discussed in this section. Finally, conclusions
134 are given in Section 5.

135

136 **2 Materials**

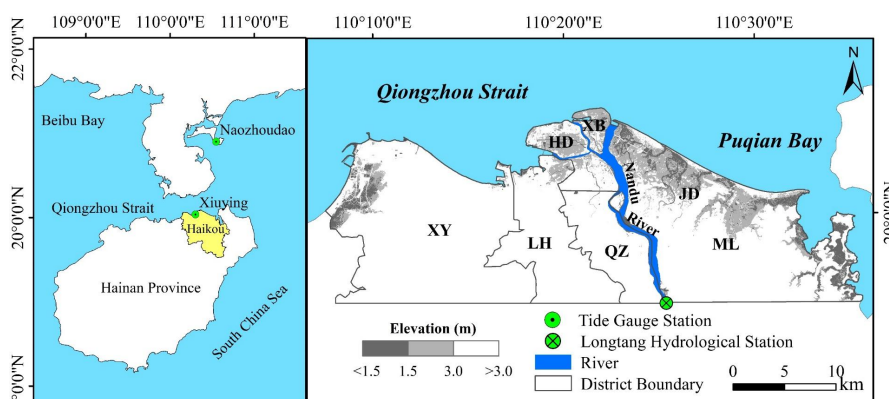
137 **2.1 Study area**

138

139 Haikou is located in the north of Hainan Island, China, where the geographical position is
140 relatively independent (Figure 1). The coastal area of Haikou is low and flat. In particular, the
141 elevation of downstream plain and areas along Nandu River (in Figure 1) is less than 3.0m.



142 Haikou is frequently affected by TCs and rainstorms from June to October, the annual rainfall is
143 around 1660 mm. Storm tide flooding caused by TCs is one of the main natural hazards in Haikou,
144 roughly 3 storm surges have occurred in Haikou every year in recent decades. The combination of
145 storm tide and rainstorm will increase the probability of extreme compound flooding, posing a
146 threat to social infrastructure and urban traffic in Haikou. During Typhoon Kalmaegi (2014), a
147 total of 219.8 mm (24h) of precipitation were produced and the highest tide level reached 4.3 m in
148 Haikou. The occurrence of heavy rainfall and strong storm tide caused serious compound flooding
149 with a 220-million-dollar economic loss. Under the changing environment, Haikou will face
150 greater compound flooding risks and challenges from TCs, storm surges, and rainstorms in the
151 future.
152



153
154 Figure 1. The geographic location of tide stations and Nandu river in Haikou, and the basic
155 geographic information of Haikou (XY: Xiuying district, LH: Longhua district, QZ: Qiongzhou
156 district, ML: Meilan district, HD: Haidian Island, XB: Xinbu Island, JD: Jiangdong New Area).
157

158 2.2 Data

159
160 The geographic and meteorological data of the study area were systematically collected in this
161 study (Table 1). The topographic map of the study area was provided by Hainan Emergency
162 Management Department, and the bathymetry data of South China Sea and Beibu Bay was
163 obtained from General Bathymetric Chart of the Oceans (GEBCO). The spatial resolution of the
164 topographic map is 5 m, and the bathymetry data is 500 m. The meteorological data includes
165 historical TC track data and daily rainfall data from 1960 to 2017. The historical TC track data
166 containing the TCs location (latitude and longitude), two-minute mean maximum sustained wind
167 (*MSW*; *m/s*), and minimum pressure (*hPa*) near the TC center, was provided by Shanghai Typhoon
168 Institute of China Meteorological Administration. The daily rainfall data of Haikou was
169 downloaded from the CMA website (<http://data.cma.cn/>), and can be transferred to hourly rainfall
170 by interpolation for inundation simulation (Ye et al., 2018; Yang et al., 2013). The annual river



171 discharges at Longtang hydrological station from 1960 to 2020 were provided by Hainan
172 Hydrology and Water Resources Survey Bureau.

173

174 Table 1. Data profile of this study

Type	Name	Attributes	Source
Basic data	DEM, Haikou	2018, 5m	Department of Emergency Management of Hainan Province
	DEM, bathymetry	2019, 500m	https://www.gebco.net
Meteorological data	TC tracks	1949-2019, 3 hourly	Shanghai Typhoon Institute of China Meteorological Administration
	Rainfall	1960-2017, daily	http://data.cma.cn
	Discharge	1960-2020, daily	Hainan Hydrology and Water Resources Survey Bureau

175

176 3 Methods

177 3.1 Model configuration and validation methods

178

179 Delft3D Flexible Mesh (DFM) developed by Deltares in 2011 is a practical unstructured shallow
180 water flow calculation model (De Goede, 2020). It can be used for both ocean hydrodynamic and
181 surface runoff numerical simulations (Kumbier et al., 2018; Meijer and Hutten, 2018). In this
182 study, the DFM model was established to calculate the hydraulic boundary conditions needed to
183 estimate overland flow boundary, and simulate the overland inundation during TCs period (Gori et
184 al., 2020b).

185 3.1.1 Storm surge model

186

187 The calculation domain of the storm surge model covers Hainan Province, the South East Sea, and
188 Beibu Bay, and roughly ranges from 15 to 24.5°N and 105.5 to 118.5°E (Figure 1). The minimum
189 mesh grid size is 100 m and the maximum mesh grid size is 12000 m. Astronomical tide is
190 simulated by importing the phase and amplitude of tidal constituents (Q1, P1, O1, K1, N2, M2, S2,
191 and K2) extracted from the global tidal model (TPX08.0). A built-in module in Delft3D WES
192 (Wind Enhance Scheme) module is employed to calculate the TCs wind field according to Holland
193 formula (Holland, 1980). We use the statistical measures *RMSE* (*Root Mean Square Error*) and *R*²
194 to evaluate the model performance of simulated tide (Kumbier et al., 2018; Skinner et al., 2015).
195 The storm surge model is validated against measured astronomical tide and storm tide
196 (astronomical tide plus storm surge). Storm tide series (TC1415, “Kalmaegi”) at Xiuying gauge
197 station were collected from Haikou Municipal Water Authority to validate this model. For the
198 validation of astronomical tide, we also collected astronomical tide for TC1415 from Xiuying and
199 Naozhoudao tide gauge station. All tide levels were recorded every hour (from 00:00 on
200 September 15, 2014 to 00:00 on September 17, 2014).



201

202 3.1.2 Overland flooding model

203

204 The overland flooding model combines regular and irregular triangular mesh. This model is a
205 surface runoff numerical model and the mesh grid resolution is set as 50 m. The average annual
206 discharge (165.81 m³/s) at Longtang hydrological station is calculated as the upstream boundary
207 condition. In this model, the storm tide series extracted from the storm surge model serve as the
208 coastal boundary conditions. This model is validated against the measured inundation area and
209 depth. We collect the inundation data of TC1415 and conduct a fieldwork of Haikou for the
210 validation of this model. By comparing the inundation map of TC1415 with measured inundation
211 area and depth, the overland inundation model can be approximately validated.

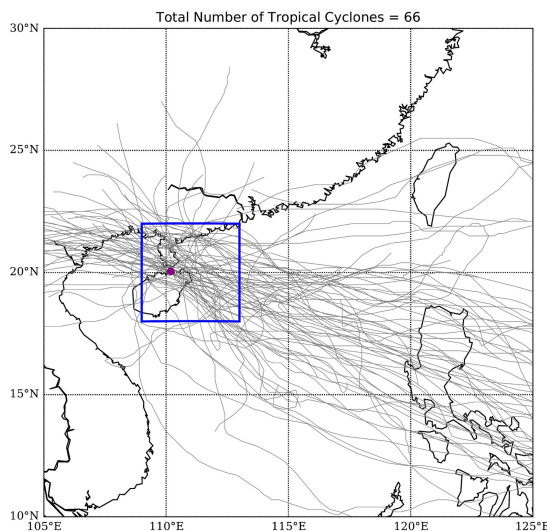
212

213 3.2 TCs influencing Haikou

214

215 The TCs that pass through the region (18-22°N, 109-113°E) and stay over 24 hours have an
216 apparent effect on Haikou (Ding, 1999; Wang, 1998; He, 1988). 66 TCs from 1960 to 2017 are
217 selected in this study (Figure 2), and we construct typhoon wind fields and simulate the storm tide
218 of these TCs. Each TC event has a code, for example, the ninth typhoon in 1963 is coded as
219 TC6309.

220



221 Figure 2. Location map for the study area. Purple dot indicates the location of Haikou. Grey
222 colored lines indicate major historical TC tracks within the region. Blue box indicates the
223 selection region (18-22°N, 109-113°E)

224

225 3.3 Compound flooding assessment

226



227 In this study, we investigate the probability distribution of storm tides to assess compound flood
228 hazards. Based on the storm surge model, the storm tide series of 66 TCs are simulated. The
229 highest storm tides during TCs are used to calculate the probability distribution function at
230 Xiuying tide gauge station.

231
232 Exploring the storm tide distribution can offer comprehension of the probability of compound
233 flood hazards from storm surge. Extreme Value Distribution (EVD) is widely applied to
234 investigate storm tide probability distribution (Yum et al., 2021). We assume that the storm tide
235 fits either Gumbel or Weibull extreme value functions, then calculate their function fitting
236 parameters. We compare the goodness-of-fit of two distribution functions (Gumbel, Weibull) with
237 Kolmogorov-Smirnov (K-S) test. K-S test is an appropriate method to explore the distribution of
238 continuous random variables, and can be used to select the best fitting distribution function.
239 According to the storm tide distribution, we can achieve tide levels at different probabilities (P).
240 We replace P with storm tide return periods (T), which equals to $1/P$, to investigate the possibility
241 of extreme storm tide. The corresponding TC events in 5-, 10-, 25-, 50-, and 100-year return
242 period can be found to compare the compound flood hazards with different storm tides.

243

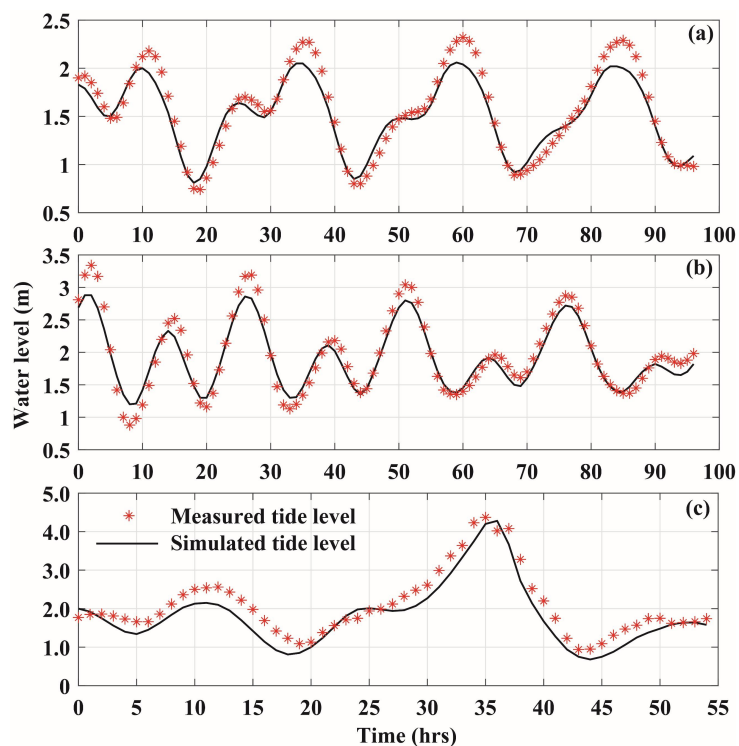
244 **4 Results and discussion**

245 **4.1 Model validation**

246

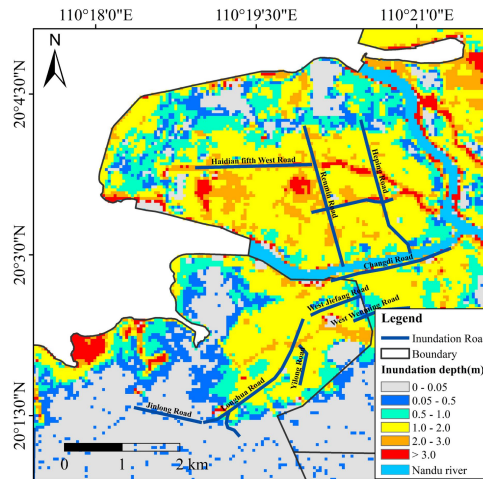
247 We use TC1415 to verify the astronomical tide and storm tide of the storm surge model. In the
248 validation of astronomical tide, we use the predicted astronomical tide at two gauge stations;
249 Naozhoudao (Zhanjiang, Guangdong) and Xiuying (Haikou, Hainan). The calculation results
250 show that the *RMSE* is 0.18 m and 0.14 m for Naozhoudao and Xiuying gauge station, the R^2 of
251 both Naozhoudao and Xiuying gauge station are 0.91. Figure 3(a) and (b) depict simulated and
252 predicted water level at Xiuying and Naozhoudao gauge station. The curves of simulated
253 astronomical tide at the two stations fit observed tide level points well. Thus, this model has a
254 good ability to simulate astronomical tides. In the validation of storm tide, we add the wind field
255 of TC1415 in the model and only use the observed tide level at Xiuying gauge station for
256 validation (Figure 3(c)). The calculation of *RMSE* is 0.34 and R^2 is 0.83. It can be seen from
257 Figure 3(c) that the curve of simulated storm tide is consistent with the observation, and the
258 highest storm tide is well simulated.

259



260
261 Figure 3. The simulation results of astronomical tide and storm tide compared to measured tide
262 levels. (a. astronomical tide at Xiuying gauge station. b. astronomical tide at Naozhoudao gauge
263 station. c. storm tide at Xiuying gauge station. Black lines indicate the simulated tide level, red
264 asterisk points indicate measured tide level.)

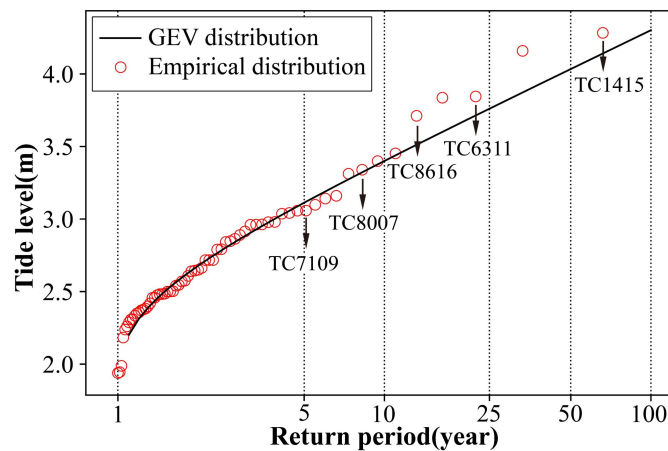
265
266 Tide levels along the coastline extracted from the storm surge model serve as coastal boundary
267 conditions for the overland flooding model. We utilize the TC1415 event to also validate the
268 overland flooding model. Comparing the simulation of compound flooding with the measured
269 inundation of roads during TC1415 (Kuang, 2014), the main inundation area in the simulation is
270 coincident with the flooded roads (Figure 4). Furthermore, the distribution of simulated inundation
271 area is also consistent with the actual flood distribution, hence this overland flooding model has
272 good capacity of modelling and demonstrating TC flood hazards.
273



274
 275 Figure 4. Spatial extent of simulated and measured inundation area and depth during TC1415.
 276

277 **4.2 Storm tide probability distribution**
 278

279 Xiuying gauge station is selected as a representative location to examine the probability
 280 exceedance of TC storm tide. Storm tide return period is calculated based on the maximum storm
 281 tide in the past 58 years simulated for 66 TCs. The results of K-S test show that the D-value and
 282 P-value of GUM are 0.0615 and 0.9995, while the D-value and P-value of WEI are 0.0769 and
 283 0.9876. Thus, the Gumbel extreme value (GEV) distribution function can fit TC storm tide better.
 284 Figure 5 shows that GEV fits storm tide well, presenting the corresponding TCs under different
 285 return periods. Red circles represent the maximum storm tide from the 66 TCs in the past. The
 286 solid line represents estimation of the GEV fitting.



287
 288 Figure 5. Storm tide at Xiuying gauge station as a function of return period based on GEV fitting
 289 (solid line).



290
291 Table 2 shows the corresponding TC events and their highest storm tide and accumulated rainfall
292 under different return periods. TC1415, with the highest storm tide, is considered a 100-year event.
293 In order to investigate the compound effects of storm tide and rainstorm on the overland
294 inundation, TCs with higher accumulated rainfall are selected. As a result, TC6311, TC8616,
295 TC8007, and TC7109 are assigned to 50, 25, 10, and 5 years based on GEV fitting, respectively.

296

297 Table 2. The different return periods of TC storm tide and the related TC events.

Return period	Event	Water level (m)	Rainfall (mm)
5Y	TC7109	3.04	137.7
10Y	TC8007	3.31	196.0
25Y	TC8616	3.71	128.0
50Y	TC6311	3.84	191.0
100Y	TC1415	4.28	219.8

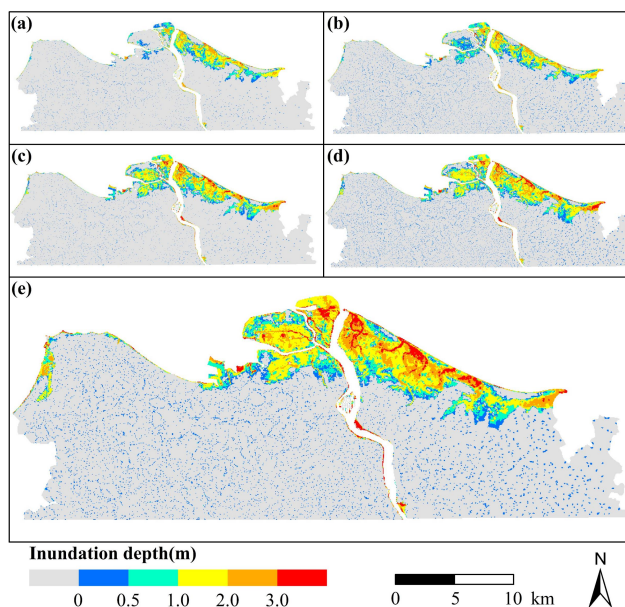
298

299 4.3 Compound flooding assessment in different storm tide return periods

300

301 Figure 6 presents the compound flood inundation maps under 5-, 10-, 25-, 50-, and 100-year
302 return period. For 5-year inundation map, the major inundation area is distributed along the
303 Jiangdong New Area and Xinbu Island on the northeast coast. The inundation area with sporadic
304 distribution is caused by rainfall in the inland urban area. As return periods increase, Haidian
305 Island, north Longhua district and northwest Xiuying district begin to have serious flood extents,
306 and the compound flooding severity of Jiangdong New Area and Xinbu Island increases. For
307 100-year return period, the inundation depth regions are above 1.0 m, and the floodplain depth is
308 above 3.0 m in most of Jiangdong New Area. Regions with inundation depth below 0.05 m are not
309 evaluated in this study due to their low risk.

310



311
 312 Figure 6. The compound flood inundation maps under different return period (a. 5-year event, b.
 313 10-year event, c. 25-year event, d. 50-year event, and e. 100-year event).
 314

315 Table 3 indicates the inundation depth and area under different return periods. In 100-year TC
 316 event, the total inundation area is 12613 ha, and the inundation area between 0-0.5 m and 1.0-2.0
 317 m accounts for 29.4% and 31.1%, respectively. The inundation area between 0.5-1.0 m and 2.0-3.0
 318 m accounts for a total of 32.7%. For the other TC events, the inundation depth at a range of 0-0.5
 319 m and 1.0-2.0 m has the most inundation area. For 100-year TC event, the inundation area with a
 320 depth above 1.0 m increases by approximately 2.5 times when compared with 5-year TC event.

321

322

Table 3. Inundation depth and area under different return periods.

Flooding depth(m)	Flooding area(ha)				
	5-year	10-year	25-year	50-year	100-year
0 – 0.5	2139	3757	2364	3957	3704
0.5 – 1.0	1349	1623	2037	1965	2065
1.0 – 2.0	1884	1980	3035	3513	3927
2.0 – 3.0	818	879	1389	1511	2055
>3.0	29	112	384	516	862
Total	6219	8351	9209	11462	12613

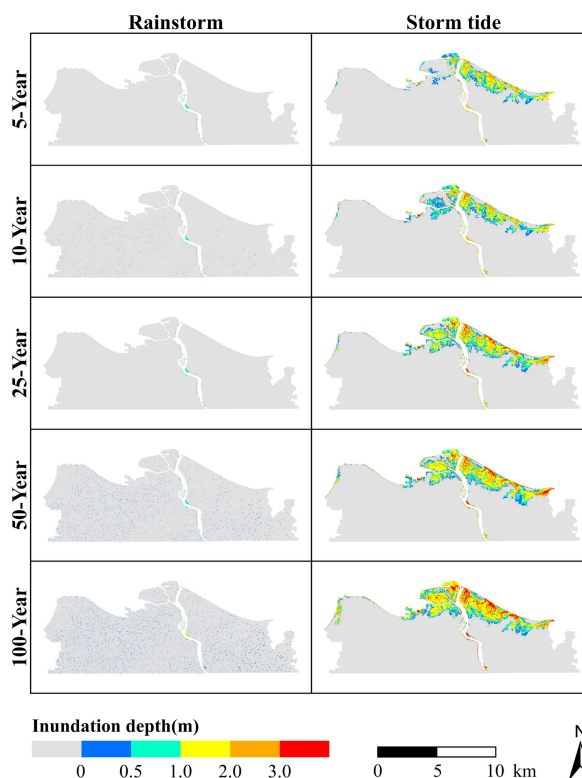
323

324 4.4 Quantitative comparison single-driven flood hazard and compound flood 325 hazard 326

327 Figure 7 illustrates the maps of rainstorm inundation and storm tide flooding under different return
 328 periods. In each rainfall scenario, the overall inundation depth is below 1.0 m, while in each storm

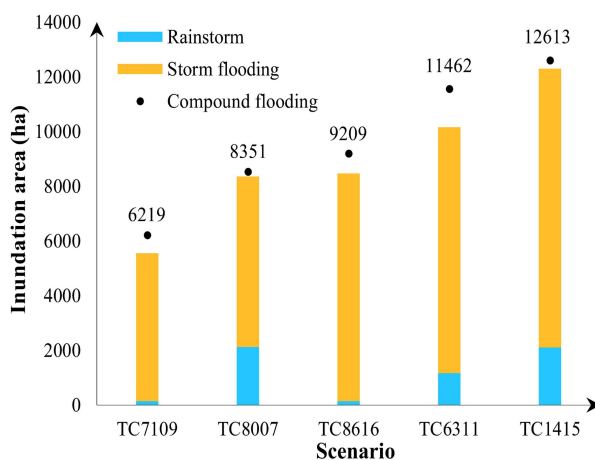


329 tide scenario, the overall inundation depth is above 1.0 m. When comparing the rainstorm
330 inundation map and storm tide flooding map in the same TC event, it is obvious that the storm tide
331 flooding is significantly worse than rainstorm inundation.



332
333 Figure 7. The inundation maps of rainstorm and storm flooding under different return periods.
334

335 Figure 8 shows the comparison of overall inundation area of rainstorm, storm tide, and compound
336 flooding under different return periods. The inundation area of compound flooding exceeds the
337 inundation area of rainstorm inundation and storm tide flooding in each TC event. Thus,
338 compound flood hazards can have more serious consequences than rainstorm and storm flooding
339 (Bevacqua et al., 2019; Wahl et al., 2015a; Zscheischler et al., 2018). Moreover, it can be seen
340 from Figure 8 that compound flooding has more inundation area than the accumulation of
341 rainstorm and storm tide flooding under different return periods. For example, in the TC6311
342 scenario, the total inundation area of compound flooding is 11462 ha, exceeding the sum of
343 rainstorm inundation and storm tide flooding, which is 10616 ha. Therefore, compound flood
344 hazards are more destructive than the combination of single-driven flood hazards, and have a
345 certain amplification effect (Fang et al., 2020; Xu et al., 2019).



346

347

Figure 8. The comparison of the overall inundation area of rainstorm, storm flooding, and compound flooding in each TC event.

348

349

350 However, storm tide and rainstorm are the driving factors in a compound flood hazard (Hsiao et
351 al., 2021; Fang et al., 2020; Bevacqua et al., 2019). In this study, we investigate the compound
352 effect of flood hazards by studying the probability distribution of highest storm tides during TCs.
353 Many studies have confirmed that rainfall and storm surge have statistically positive dependence
354 (Wahl et al., 2015; Xu et al., 2014; Zheng et al., 2014). Hence, it is of practical significance to
355 reveal compound flood risk considering the statistical dependence of rainfall and storm surge.
356 Copula function has been confirmed that to not only model and describe the dependence between
357 flood variables, but also to express compound flood risk (Zellou and Rahali, 2019; Xu et al., 2019;
358 Wu et al., 2018; Lian et al., 2013b). In future works, we will adopt the copula function to
359 investigate the joint occurrence of rainfall and storm surge during TCs, further assessing extreme
360 compound flooding severity.

361

362 5 Conclusions

363

364 This study applies a coupled methodology of combining storm surge model and overland flooding
365 model to investigate the compound effect of flood hazards during TCs. We simulate and assess
366 compound floods under different return periods of storm tides. The results show that storm tide is
367 the key driving factor of compound flood inundation in Haikou, and tide level decides the
368 inundation extent. When quantitatively comparing compound flooding with rainstorm inundation
369 and storm flooding, we find that it is more destructive than single-driven flood hazards, and the
370 compound effect exceeds the accumulated effects of single-driven floods. The co-occurrence of
371 heavy rainfall and strong storm surge in extreme TCs could intensify compound flood inundation.
372 Simply accumulating every single-driven flood hazard to define compound flooding may cause



373 underestimation.

374

375 Although this study is limited to Haikou City, the methodology of quantitatively assessing
376 compound flooding risks through constructing a coupled framework of two hydrodynamic models
377 is available for other coastal cities. It can conveniently capture the dynamic of rainfall and storm
378 surge, and directly observe the change of inundation area to display the effect of rainfall and storm
379 surge in compound events. For future research on extreme TC compound flooding, copula
380 function can be applied to study the statistical dependence between heavy rainfall and strong
381 storm surge, revealing extreme flood risk in coastal cities.

382

383 **Data availability**

384 Some of the used data such as the typhoon tracks in this study are freely available. The web links
385 are presented in Section 2. However, some data such as the topology map of the study area and
386 river discharges were provided on the request from the departments and agencies of Haikou.

387

388 **Author contribution**

389 QL, HQX and JW designed the study. QL construct and validated the models, and ran all the
390 simulations. QL and HQX analyzed and interpreted the results. QL wrote, reviewed, and edited the
391 manuscript. HQX and JW reviewed the manuscript.

392

393 **Competing interests**

394 The authors declare that they have no conflict of financial interest that could have appeared to
395 influence the work reported in this paper.

397

398 **Acknowledgements**

399 The authors express gratitude to the Department of Emergency Management of Hainan Province
400 Hainan Hydrology and Water Resources Survey Bureau for supporting the geographic information
401 of the study area. This work was supported by the National Key Research and Development
402 Program of China (2018YFC1508803), and the National Social Science Foundation of China
403 (18ZDA105).

405



406 **References**

- 407 Adelekan, I.O.: Vulnerability assessment of an urban flood in Nigeria: Abeokuta flood 2007. *Nat.*
408 *Hazards*, 56, 215–231, <https://doi.org/10.1007/s11069-010-9564-z>, 2011.
- 409 Bevacqua, E., Maraun, D., Vousdoukas, M., et al: Higher probability of compound flooding from
410 precipitation and storm surge in Europe under anthropogenic climate change. *Sci. Adv.*, 5,
411 eaaw5531, <https://doi.org/10.1126/sciadv.aaw5531>, 2019.
- 412 Bilskie, M., Zhao, H., Resio, D., et al.: Enhancing Flood Hazard Assessments in Coastal Louisiana
413 Through Coupled Hydrologic and Surge Processes. *Frontiers in Water*, 3, 609231,
414 <https://doi.org/10.3389/frwa.2021.609231>, 2021.
- 415 Budiyono, Y., Aerts, J., Tollenaar, D., et al.: River flood risk in Jakarta under scenarios of future
416 change. *Nat. Hazards Earth Syst. Sci.*, 16, 757–774,
417 <https://doi.org/10.5194/nhess-16-757-2016>, 2016.
- 418 De Goede, E.: Historical overview of 2D and 3D hydrodynamic modelling of shallow water flows
419 in the Netherlands. *Ocean Dyn.*, 70, 521–539, <https://doi.org/10.1007/s10236-019-01336-5>,
420 2020.
- 421 Deltares. D-Flow Flexible Mesh - (RGFGRID). Deltares, 2018.
- 422 Ding, Q.: Analysis and forecast of storm surges in Haikou harbor. *Marine Forecasts*, 16(1): 41-47,
423 1999. (in Chinese)
- 424 Emanuel, K.: Assessing the present and future probability of Hurricane Harvey’s rainfall. *Proc.*
425 *Natl. Acad. Sci.*, 114, 12681–12684, <https://doi.org/10.1073/pnas.1716222114>, 2017.
- 426 Fang, J., Wahl, T., Fang, J., et al.: Compound flood potential from storm surge and heavy
427 precipitation in coastal China (preprint). *Hydrometeorology/Stochastic approaches*,
428 <https://doi.org/10.5194/nhess-2020-377>, 2020.
- 429 Gori, A., Lin, N., Smith, J.: Assessing compound flooding from landfalling tropical cyclones on
430 the North Carolina coast. *Water Resour. Res.*, 56, <https://doi.org/10.1029/2019WR026788>,
431 2020a.
- 432 Gori, A., Lin, N., Xi, D.: Tropical cyclone compound flood hazard assessment: from investigating
433 drivers to quantifying extreme water levels. *Earths Future*, 8,
434 <https://doi.org/10.1029/2020EF001660>, 2020b.
- 435 Hallegatte, S., Green, C., Nicholls, R., et al.: Future flood losses in major coastal cities. *Nat. Clim.*
436 *Change*, 3, 802–806, <https://doi.org/10.1038/nclimate1979>, 2013.
- 437 He, F., Hu, H., Dong, G., et al.: Compound flooding simulation and prediction of future recurrence
438 in Shanghai downtown area. *Journal of Catastrophology*, 35(4): 93-98, 134, 2020. (in
439 Chinese)
- 440 He, H.: Storm surges along the coast of Guangdong and Hainan. *Tropical Oceanology*, (2): 39-46,
441 1988. (in Chinese)
- 442 Hendry, A., Haigh, I., Nicholls, R., et al.: Assessing the characteristics and drivers of compound
443 flooding events around the UK coast. *Hydrol. Earth Syst. Sci.*, 23, 3117–3139,



- 444 <https://doi.org/10.5194/hess-23-3117-2019>, 2019.
- 445 Holland, G.: An Analytic Model of the Wind and Pressure Profiles in Hurricanes. *Monthly*
446 *Weather Review.*, 108(8): 1218-1218, 1980.
- 447 Hsiao, S., Chiang, W., Jang, J., et al.: Flood risk influenced by the compound effect of storm surge
448 and rainfall under climate change for low-lying coastal areas. *Sci. Total Environ.*, 764,
449 144439, <https://doi.org/10.1016/j.scitotenv.2020.144439>, 2021.
- 450 Huang, W., Ye, F., Zhang, Y., et al.: Compounding factors for extreme flooding around Galveston
451 Bay during Hurricane Harvey. *Ocean Model.*, 158, 101735,
452 <https://doi.org/10.1016/j.ocemod.2020.101735>, 2021.
- 453 Keellings, D., Hernández Ayala, J.: Extreme Rainfall Associated with Hurricane Maria Over
454 Puerto Rico and Its Connections to Climate Variability and Change. *Geophys. Res. Lett.*, 46,
455 2964–2973, <https://doi.org/10.1029/2019GL082077>, 2019.
- 456 Kumbier, K., Carvalho, R., Vafeidis, A., et al.: Investigating compound flooding in an estuary
457 using hydrodynamic modelling: a case study from the Shoalhaven River, Australia. *Nat.*
458 *Hazards Earth Syst. Sci.*, 18, 463–477, <https://doi.org/10.5194/nhess-18-463-2018>, 2018.
- 459 Kuang, C., Zhang, G.: How can cities practice to have a great drainage system? *Daily Hainan A04*,
460 2014. (in Chinese)
- 461 Lian, J., Xu, H., Xu, K., et al.: Optimal management of the flooding risk caused by the joint
462 occurrence of extreme rainfall and high tide level in a coastal city. *Nat. Hazards*, 89, 183–200,
463 <https://doi.org/10.1007/s11069-017-2958-4>, 2017.
- 464 Lian, J., Xu, K., Ma, C.: Joint impact of rainfall and tidal level on flood risk in a coastal city with
465 a complex river network: a case study of Fuzhou City, China. *Hydrol. Earth Syst. Sci.*, 17,
466 679–689, <https://doi.org/10.5194/hess-17-679-2013>, 2013.
- 467 Lin, N., Emanuel, K., Oppenheimer, M.: Physically based assessment of hurricane surge threat
468 under climate change. *Nature Clim Change*, 2, 462–467,
469 <https://doi.org/10.1038/nclimate1389>, 2012.
- 470 Marsooli, R., Lin, N., Emanuel, K.: Climate change exacerbates hurricane flood hazards along US
471 Atlantic and Gulf Coasts in spatially varying patterns. *Nat Commun.*, 10, 3785,
472 <https://doi.org/10.1038/s41467-019-11755-z>, 2019.
- 473 Milly, P., Wetherald, R., Dunne, K. et al.: Increasing risk of great floods in a changing climate.
474 *Nature*, 415, 514–517, <https://doi.org/10.1038/415514a>, 2002.
- 475 Orton, P., Conticello, F., Cioffi, F., et al.: Flood hazard assessment from storm tides, rain and sea
476 level rise for a tidal river estuary. *Nat. Hazards*, 102, 729–757,
477 <https://doi.org/10.1007/s11069-018-3251-x>, 2020.
- 478 Patricola, C., Wehner, M.: Anthropogenic influences on major tropical cyclone events. *Nature*, 563,
479 339–346, <https://doi.org/10.1038/s41586-018-0673-2>, 2018.
- 480 Rasmussen, D., Bittermann, K., Buchanan, M., et al.: Coastal flood implications of 1.5 °C, 2.0 °C,
481 and 2.5 °C temperature stabilization targets in the 21st and 22nd century. 2017.



- 482 Santiago-Collazo, F., Bilskie, M., Hagen, S.: A comprehensive review of compound inundation
483 models in low-gradient coastal watersheds. *Environ. Model. Softw.*, 119, 166–181,
484 <https://doi.org/10.1016/j.envsoft.2019.06.002>, 2019.
- 485 Shen, Y., Morsy, M., Huxley, C., et al.: Flood risk assessment and increased resilience for coastal
486 urban watersheds under the combined impact of storm tide and heavy rainfall. *J. Hydrol.*, 579,
487 124159, <https://doi.org/10.1016/j.jhydrol.2019.124159>, 2019.
- 488 Valle-Levinson, A., Olabarieta, M., Heilman, L.: Compound flooding in Houston-Galveston Bay
489 during Hurricane Harvey. *Sci. Total Environ.*, 747, 141272,
490 <https://doi.org/10.1016/j.scitotenv.2020.141272>, 2020.
- 491 van Oldenborgh, G., van der Wiel, K., Sebastian, A., et al.: Attribution of extreme rainfall from
492 Hurricane Harvey, August 2017. *Environ. Res. Lett.*, 12, 124009,
493 <https://doi.org/10.1088/1748-9326/aa9ef2>, 2017.
- 494 Wahl, T., Jain, S., Bender, J., et al.: Increasing risk of compound flooding from storm surge and
495 rainfall for major US cities. *Nat. Clim. Change*, 5, 1093–1097,
496 <https://doi.org/10.1038/nclimate2736>, 2015.
- 497 Wang, H., Lu, H., Yu, X.J., et al.: Analysis storm surge's characteristics along the coast of Hainan
498 Island. *Marine Forecasts*, 15(2): 34-42, 1998. (in Chinese)
- 499 Wang, J., Tan, J.: Understanding the climate change and disaster risks in coastal areas of China to
500 develop coping strategies. *Progress in Geography*, 40(5): 870-882, 2021. (in Chinese)
- 501 Wang, L., Zhang, M., Wen, J., et al.: Simulation of extreme compound coastal flooding in
502 Shanghai. *Advance in Water Science*, 30(4): 546-555, 2020. (in Chinese)
- 503 Wang, J., Gao, W., Xu, S., et al.: Evaluation of the combined risk of sea level rise, land subsidence,
504 and storm surges on the coastal areas of Shanghai, China. *Clim. Change*, 115, 537–558,
505 <https://doi.org/10.1007/s10584-012-0468-7>, 2012.
- 506 Wang, J., Yi, S., Li, M., et al.: Effects of sea level rise, land subsidence, bathymetric change and
507 typhoon tracks on storm flooding in the coastal areas of Shanghai. *Sci. Total Environ.*, 621,
508 228–234, <https://doi.org/10.1016/j.scitotenv.2017.11.224>, 2018.
- 509 Wu, W., McInnes, K., O'Grady, J., et al.: Mapping Dependence Between Extreme Rainfall and
510 Storm Surge. *J. Geophys. Res. Oceans*, 123, 2461–2474,
511 <https://doi.org/10.1002/2017JC013472>, 2018.
- 512 Xu, H., Xu, K., Bin, L., et al.: Joint Risk of Rainfall and Storm Surges during Typhoons in a
513 Coastal City of Haidian Island, China. *Int. J. Environ. Res. Public Health*, 15, 1377,
514 <https://doi.org/10.3390/ijerph15071377>, 2018.
- 515 Xu, H., Xu, K., Lian, J., et al.: Compound effects of rainfall and storm tides on coastal flooding
516 risk. *Stoch. Environ. Res. Risk Assess*, 33, 1249–1261,
517 <https://doi.org/10.1007/s00477-019-01695-x>, 2019.
- 518 Xu, K., Ma, C., Lian, J., et al.: Joint Probability Analysis of Extreme Precipitation and Storm Tide
519 in a Coastal City under Changing Environment. *PLoS ONE*, 9, e109341.



- 520 <https://doi.org/10.1371/journal.pone.0109341>, 2014.
- 521 Yang, X., Zhu, D., Li, C., et al.: Establishment of design hyetographs based on risk probability
522 models. *Journal of Hydraulic Engineering*, 44(5): 542-548, 2013. (in Chinese)
- 523 Ye, S., Ye, X., Wang, Y., et al.: Research on design rainstorm pattern based on Copula function.
524 *Journal of Water Resources & Water Engineering*, 29(3): 63-68, 2018. (in Chinese)
- 525 Yin, J., Lin, N., Yang, Y., et al.: Hazard Assessment for Typhoon - Induced Coastal Flooding and
526 Inundation in Shanghai, China. *J. Geophys. Res. Oceans*, 126,
527 <https://doi.org/10.1029/2021JC017319>, 2021.
- 528 Yin, J., Yu, D., Yin, Z., et al.: Evaluating the impact and risk of pluvial flash flood on intra-urban
529 road network: A case study in the city center of Shanghai, China. *J. Hydrol.*, 537, 138–145,
530 <https://doi.org/10.1016/j.jhydrol.2016.03.037>, 2016.
- 531 Yin, J., Yu, D., Yin, Z., et al.: Modelling the combined impacts of sea-level rise and land
532 subsidence on storm tides induced flooding of the Huangpu River in Shanghai, China. *Clim.*
533 *Change*, 119, 919–932, <https://doi.org/10.1007/s10584-013-0749-9>, 2013.
- 534 Yum, S., Wei, H., Jang, S.: Estimation of the non-exceedance probability of extreme storm surges
535 in South Korea using tidal-gauge data. *Nat. Hazards Earth Syst. Sci.*, 21, 2611–2631,
536 <https://doi.org/10.5194/nhess-21-2611-2021>, 2021.
- 537 Zellou, B., Rahali, H. Assessment of the joint impact of extreme rainfall and storm surge on the
538 risk of flooding in a coastal area. *J. Hydrol.*, 569, 647–665,
539 <https://doi.org/10.1016/j.jhydrol.2018.12.028>, 2019.
- 540 Zheng, F., Westra, S., Leonard, M., et al.: Modeling dependence between extreme rainfall and
541 storm surge to estimate coastal flooding risk. *Water Resour. Res.*, 50, 2050–2071,
542 <https://doi.org/10.1002/2013WR014616>, 2014.
- 543 Zscheischler, J., Westra, S., van den Hurk, B., et al.: Future climate risk from compound events.
544 *Nat. Clim. Change*, 8, 469–477, <https://doi.org/10.1038/s41558-018-0156-3>, 2018.
- 545